Inorganic Chemistry

Article

pubs.acs.org/IC

Terms of Use

# Lanthanide Loading of Luminescent Multi-Tridentate Polymers under Thermodynamic Control

Lucille Babel,[†,§] Thi Nhu Y Hoang,[†,§] Homayoun Nozary,[†] Jasmina Salamanca,[†] Laure Guénée,[‡] and Claude Piguet*[,†]

[†]Department of Inorganic, Analytical and Applied Chemistry, University of Geneva, 30 quai E. Ansermet, CH-1211 Geneva 4, Switzerland

[‡]Laboratory of Crystallography, University of Geneva, 24 quai E. Ansermet, CH-1211 Geneva 4, Switzerland

Supporting Information

**ABSTRACT:** This work illustrates the use of basic statistical mechanics for rationalizing the loading of linear multitridentate polymers with trivalent lanthanides, Ln(III), and identifies the specific ionic sizes of europium and yttrium as promising candidates for the further design of organized heterometallic f–f′ materials. Using $[Ln(hfac)_3]$ (hfac = hexafluoroacetylacetonate) as lanthanide carriers, the thermodynamically controlled formation of Wolf type-II lanthanidopolymers $[\{Ln(hfac)_3\}_m(\mathbf{L4})]$ is modeled with the help of two simple microscopic descriptors: (i) the intrinsic affinity of Ln(III) for the tridentate binding sites $f_{N3}^{Ln}$ and (ii) the intermetallic interactions $\Delta E_{1-2}^{Ln,Ln}$ operating between two occupied adjacent sites. Selective complexation ($f_{N3}^{La} \ll f_{N3}^{Eu} > f_{N3}^{Y}$) modulated by anticooperative interactions ($\Delta E_{1-2}^{La,La} \simeq \Delta E_{1-2}^{Eu,Eu} > \Delta E_{1-2}^{Y,Y} \approx 0$) favors the fixation of Eu(III) in semiorganized lanthanidopolymers $[\{Eu(hfac)_3\}_m(\mathbf{L4})]$ displaying exploitable light-downshifting.

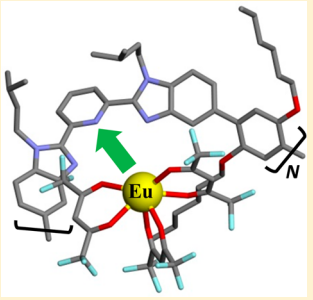


## INTRODUCTION AND THEORETICAL BACKGROUND

Since the turn of the nineteenth century, macroscopic lanthanide-containing crystals,[1] solids, and alloys found a wealth of technological applications,[2] especially as catalysts for chemical transformations,[3] as phosphors for lighting,[4] and as primary components in magnets[5] and in supra- and superconductors.[6] In contrast, the development of discrete molecular lanthanide complexes working as microscopic optical and magnetic devices was delayed by the difficult acceptance of their preferences for coordination numbers larger than six.[7] After two decades, a plethora of well-defined mono- and polynuclear microscopic lanthanide-containing architectures have been designed for being used as luminescent probes and (bio)sensors,[8] as contrasts agents for magnetic resonance imaging,[9] as single-molecule magnets, and as spin qubits.[10] The recent need for lanthanide-containing entities, the sizes of which being intermediate between molecules and bulk materials,[11,12] relies either on the miniaturization of macroscopic solids to give optically active nanoparticles improving solar cell technologies[11] or on the integration of discrete luminescent lanthanide complexes into hybrid materials.[12]

Surprisingly, the alternative design of *lanthanidopolymers*, i.e., lanthanide-loaded organic polymers, is comparatively much less developed, probably as a result of their difficult characterization and their elusive structures, in which the degree of metal occupancy varies in an uncontrolled way upon minor changes in the external conditions (solvents, temperature, stoichiometry).[13] Following Wolf's concept depicted in Scheme 1,[14] metallopolymers can be classified according to the strength of the electronic communication between the organic backbone and the metals. In type I metallopolymers, the metal complexes are easily tethered to the organic support, but they poorly benefit from the electronic properties of the backbone, while for type III, the crucial contribution of the metallic cations to the polymeric network prevents minimum tuning and adaptation. Though synthetically more demanding, Wolf type II metallopolymers represent an ideal case, where the toolbox of coordination chemistry combined with basic statistical mechanics should allow the rational loading of linear multisite receptors **L** with trivalent lanthanides, Ln(III),[1] according to eq 1 (Figure 1a).

**Scheme 1. Wolf Type I–III Strategies for the Introduction of Lanthanide-Binding Sites into Organic Polymers[14a]**

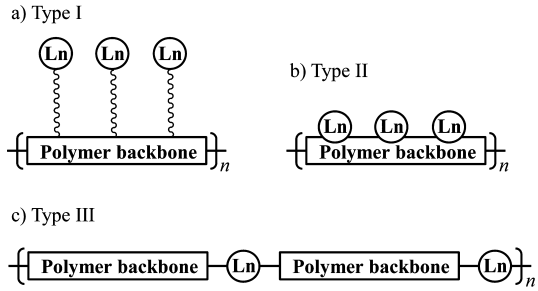


[a]The chelating units are (a) connected to the periphery (type I), (b) incorporated within the polymer backbone (type II), and (c) integrated as components of the polymer backbone (type III).

**Received:** December 12, 2013
**Published:** January 20, 2014

   dx.doi.org/10.1021/ic4030525 | *Inorg. Chem.* 2014, 53, 3568–3578

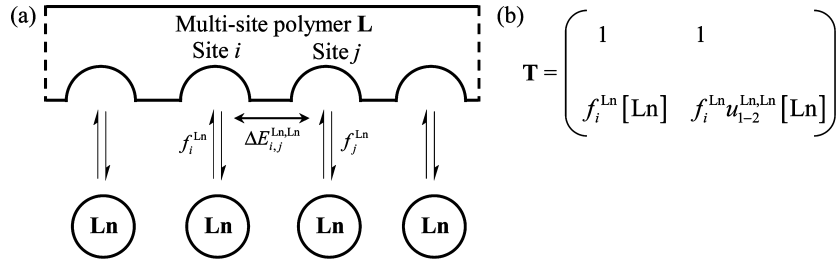


**Figure 1.** (a) Thermodynamic model and (b) associated transfer matrix used for modeling the successive intermolecular connections of lanthanide ions to the one-dimensional multisite receptor **L**. $f_i^{Ln}$ and $\Delta G_i^{Ln} = -RT\ln(f_i^{Ln})$ are the intrinsic affinity and free energy of connection of site $i$ for the entering metal, respectively, and $\Delta E_{i,j}^{Ln,Ln}$ is the free energy of interaction occurring when two adjacent sites $i$ and $j$ are occupied.

$$\mathbf{L} + m\mathrm{Ln}^{3+} \rightleftharpoons [\mathrm{Ln}_m\mathbf{L}]^{3m+}\ \beta_{m,1}^{\ln,\mathbf{L}} \tag{1}$$

Any macrospecies $[\mathrm{Ln}_m\mathbf{L}]^{3m+}$ is composed of numerous microspecies $\{\boldsymbol{s}_i\}$−$[\mathrm{Ln}_m\mathbf{L}]^{3m+}$, all possessing the same number $m$ of metals bound to the receptor but differing on their exact location in the various sites as described by the state vector $\{\boldsymbol{s}_i\}$ for which each element $s_i = 1$ indicates that a metal is bound to site $i$ and $s_i = 0$ when no metal is coordinated. With the help of the two simple microscopic descriptors $f_i^{Ln}$ and $\Delta E_{i,j}^{Ln,Ln}$ illustrated in Figure 1a (i.e., $f_i^{Ln}$ is the intrinsic affinity of site $i$ for the entering metal and $\Delta E_{i,j}^{Ln,Ln}$ is the free energy of interaction occurring when two adjacent sites $i$ and $j$ are occupied), the Ising model limited to near-neighbor interactions associates a stability microconstant $\beta_{m,1}^{Ln,L}\{s_i\}$ to each $\{\boldsymbol{s}_i\}$-$[\mathrm{Ln}_m\mathbf{L}]^{3m+}$ microspecies where **L** possesses $N$ available binding sites (eq 2; see Appendix 1 for details). The sum of the microconstants $\beta_{m,1}^{Ln,L} = \sum_{\{s_i\}}\beta_{m,1}^{Ln,L}\{\boldsymbol{s}_i\}$ corresponds to the target macroconstant considered in eq 1.[15]

$$\beta_{m,1}^{Ln,L}\{s_i\} = \prod_{i=1}^{N}(f_i^{Ln})^{s_i}\cdot\sqrt{\prod_{i=1}^{N}\prod_{j\neq i}^{N}[\exp(-\Delta E_{i,j}^{Ln,Ln}/RT)]^{s_i s_j}} \tag{2}$$

Broad scope chemists may be rightfully frightened by the rigorous formulation shown in eq 2, but its practical application is rather intuitive. Let us limit the size of the receptor to three adjacent sites ($N = 3$) in $\mathbf{L}^3$, labeled $t$(erminal)−$c$(entral)−$t$(erminal), in brief *tct*. When all three sites are occupied by metallic cations, $t^1c^1t^1$ is the only microspecies contributing to $[\mathrm{Ln}_3\mathbf{L}^3]$ (eq 1). The application of eq 2 provides the stability constant $\beta_{3,1}^{Ln,L^3} = \beta_{3,1}^{Ln,L}\{t^1c^0t^1\} = (f_i^{Ln})^3[\exp(-\Delta E_{c,t}^{Ln,Ln}/RT)]^2 = (f_i^{Ln})^3(u_{c,t}^{Ln,Ln})^2$, which simply corresponds to thrice the intermolecular Ln−site $i$ connection $(f_i^{Ln})^3$; i.e., each site is occupied by a metal in $t^1c^1t^1$, modulated by twice the adjacent Ln···Ln interaction $(u_{c,t}^{Ln,Ln})^2$, taken as its Boltzmann factor $u_{c,t}^{Ln,Ln} = \exp(-\Delta E_{c,t}^{Ln,Ln}/RT)$. When only two sites are occupied by lanthanide cations in $[\mathrm{Ln}_2\mathbf{L}^3]$, one obviously counts only two Ln−site $i$ connections $(f_i^{Ln})^2$ with no adjacent intermetallic interaction for the $t^1c^0t^1$ microspecies, i.e., $\beta_{2,1}^{Ln,L^3}\{t^1c^0t^1\} = (f_i^{Ln})^2$, but modulated by a single intermetallic interaction for the alternative doubly degenerate $t^1c^1t^0 \equiv t^0c^1t^1$ microspecies, i.e., $\beta_{2,1}^{Ln,L^3}\{t^1c^0t^1\} = 2(f_i^{Ln})^2u_{c,t}^{Ln,Ln}$. Summing over the three microspecies eventually gives $\beta_{2,1}^{Ln,L^3} = (f_i^{Ln})^2(1 + 2u_{c,t}^{Ln,Ln})$ for the $[\mathrm{Ln}_2\mathbf{L}^3]$ macrospecies. Finally, the fixation of a single metal to the receptor in $[\mathrm{Ln}\mathbf{L}^3]$ gives the triply degenerate $t^1c^0t^0 \equiv t^0c^1t^0 \equiv t^0c^0t^1$ microspecies characterized by a single Ln−site $i$ connection, the macroconstant of which is given by $\beta_{1,1}^{Ln,L^3} = 3f_i^{Ln}$.[16] To summarize, any cumulative stability constant $\beta_{m,1}^{Ln,L}$ associated with a macroscopies can be modeled by a straightforward enumeration of its contributing microspecies, each being represented by their numbers of occupied sites $(f_i^{Ln})^m$ and of adjacent intermetallic interactions $(u_{i,j}^{Ln,Ln})^n$. Statistical mechanics generalizes this intuitive approach for any number $N$ of binding sites with the help of the semigrand partition function $\Xi$, introduced by Wyman as the binding polynomial $\sum_{m=0}^{N}\beta_{m,1}^{Ln,L}[\mathrm{Ln}]^m$, where [Ln] is the activity of the free lanthanide in solution (eq 3, left-hand side).[17] This partition function is actually more efficiently computed by using the transfer matrix formalism written on the right-hand side of eq 3, where **T** is the tranfer matrix adapted to the Ising model shown in Figure 1b, $V_g = \begin{pmatrix}1\\0\end{pmatrix}$, $\tilde{V}_t = (1\ 1)$ are the generating and transposed terminating vectors, respectively (see Appendix 1 for details).[15]

$$\Xi = \sum_{m=0}^{N}\beta_{m,1}^{Ln,\mathbf{L}}[\mathrm{Ln}]^m = \tilde{V}_t\mathbf{T}^N V_g \tag{3}$$

Applied to our working example, which considers a receptor with $N = 3$, eq 3 yields

$$\begin{aligned}\Xi &= \sum_{m=0}^{3}\beta_{m,1}^{Ln,L^3}[\mathrm{Ln}]^m \\ &= (1\ 1)\begin{pmatrix}1 & 1\\ f_i^{Ln}[\mathrm{Ln}] & f_i^{Ln}u^{Ln,Ln}[\mathrm{Ln}]\end{pmatrix}^3\begin{pmatrix}1\\0\end{pmatrix} \\ &= 1 + 3f_i^{Ln}[\mathrm{Ln}] + (f_i^{Ln})^2(1 + 2u^{Ln,Ln})[\mathrm{Ln}]^2 \\ &\quad + (f_i^{Ln})^3(u^{Ln,Ln})^2[\mathrm{Ln}]^3\end{aligned} \tag{4}$$

Comparison of the transfer matrix calculation (eq 4, right-hand side) with the binding polynomial (eq 4, left-hand side) provides the cumulative macroconstants $\beta_{m,1}^{Ln,L^3}$ ($m = 1$−3) previously derived by intuition. We are thus equipped for modeling any metal loading process operating in a Wolf type-II metallopolymer with the simple resort to the free energy of metal-binding site affinity $\Delta G_i^{Ln} = -RT\ln(f_i^{Ln})$ and the intermetallic interactions $\Delta E_{1-2}^{Ln,Ln}$ operating between two adjacent occupied sites.[18] The sign of the latter parameter is crucial for the deliberate metal loading of the polymer.[17] A purely statistical distribution of the metals among the various sites is predicted for $\Delta E_{1-2}^{Ln,Ln} \approx 0$, but $\Delta E_{1-2}^{Ln,Ln} < 0$ produces metal clustering whereas $\Delta E_{1-2}^{Ln,Ln} > 0$ results in the alternation of free and occupied sites, the latter situation being highly desired for the preparation of heterometallic luminescent lanthanide-containing materials[17b,19] displaying controlled


dx.doi.org/10.1021/ic4030525 | Inorg. Chem. 2014, 53, 3568−3578

**Scheme 2. Chemical Structures of the Ligands L1−L4**

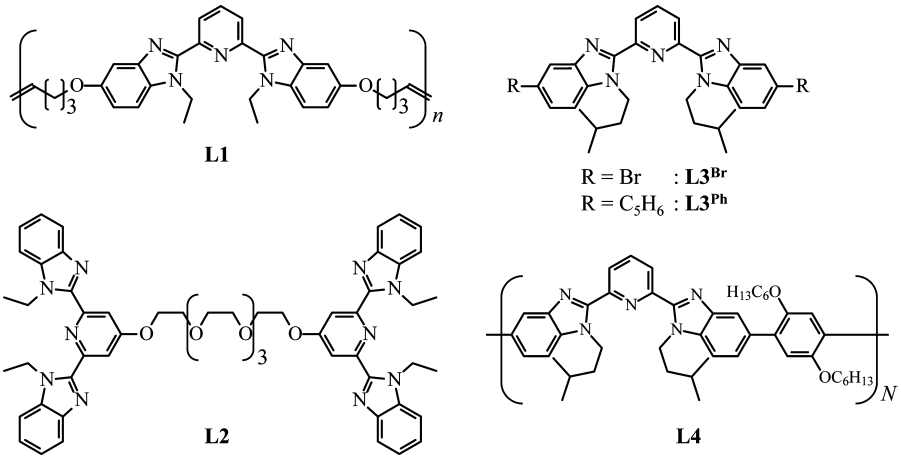


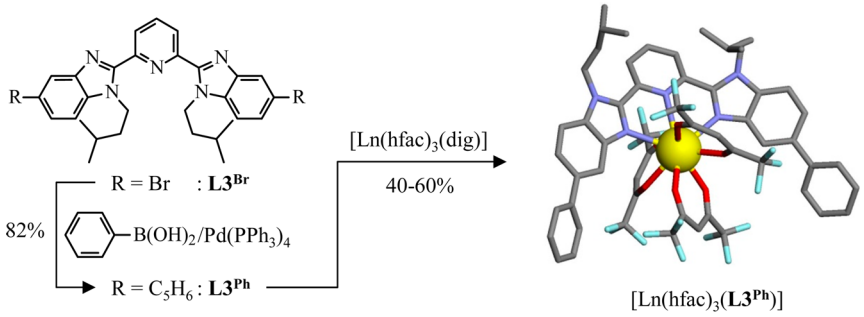


**Figure 2.** Synthesis of ligand $\mathbf{L3^{Ph}}$ and of its mononuclear complexes $[Ln(hfac)_3(\mathbf{L3^{Ph}})]$. A perspective view of the X-ray diffraction molecular structure of $[La(hfac)_3(\mathbf{L3^{Ph}})]$ is shown on the right.

intramolecular energy transfer processes.[4,20] However, the level of understanding and prediction of $\Delta E_{1-2}^{Ln,Ln}$ is hampered by the underlying competition between intramolecular electrostatic intermetallic repulsion and solvation processes,[21] and no rational approach is currently available for planning repulsive intermetallic interactions (i.e., $\Delta E_{1-2}^{Ln,Ln} > 0$) in uncharged single-stranded Wolf type-II metallopolymers.

Inspired by the pioneering empirical preparation of flexible luminescent lanthanidopolymers with **L1** (type II)[22] and **L2** (type III),[23] we report here on the connection of related lipophilic tridentate 2,6-bis(benzimidazol-2-yl)pyridine binding units **L3** to rigid 1-4-phenyl spacers to give rigid linear polymers **L4**, where a single $\Delta E_{1-2}^{Ln,Ln}$ parameter operates (Scheme 2).[24] The thermodynamic control of the lanthanide loading and the emergence of remarkable binding selectivities in solution are deduced from the characterization and the modeling of the complexation reactions between **L4** and $[Ln(hfac)_3(dig)]$ (Ln = La, Eu, Y; hfac = hexafluoroacetylacetonate; dig = diglyme = 1-methoxy-2-(2-methoxyethoxy)-ethane),[25] whereas downshifted luminescence is analyzed in terms of occupancy factors and metal distributions when Ln = Eu.

## RESULTS AND DISCUSSION

**Synthesis, Characterization, and Thermodynamic Behavior of the Lanthanidomonomers $[Ln(hfac)_3(\mathbf{L3^{Ph}})]$.** The polyaromatic ligand $\mathbf{L3^{Ph}}$ is synthesized from the dibromo derivative $\mathbf{L3^{Br}}$[25a] according to a Miyaura−Suzuki strategy (Figure 2).[24] Reactions with the neutral complexes $[Ln(hfac)_3(dig)]$ (Ln = La, Eu, Y)[26] give 40−60% of the mononuclear complexes $[Ln(hfac)_3(\mathbf{L3^{Ph}})]$ as crystalline materials, in which the central lanthanide cation[1] is nine-coordinated in a distorted monocapped square-antiprism, the nitrogen atom of the central pyridine ring occupying the capping position as previously reported for $[Ln(hfac)_3(\mathbf{L3^{Br}})]$ (Figure 2 and Appendix 2).[25a]

The molecular structure of $[La(hfac)_3(\mathbf{L3^{Ph}})]$ in the crystal structure of $[La(hfac)_3(\mathbf{L3^{Ph}})]\cdot 0.34\ CH_3CN$ (Figure S1) is almost superimposable with that of $[La(hfac)_3(\mathbf{L3^{Br}})]$, except for the replacement of the slight helical twist characterizing the ligand strand in the latter complex with a butterfly conformation in $[La(hfac)_3(\mathbf{L3^{Ph}})]$ (Figure S2). In $CD_2Cl_2$ solution, the 12 $^1H$ NMR signals observed for the protons (H1−H12) of the ligand are diagnostic for the meridional tricoordination of $\mathbf{L3^{Ph}}$ (Figure 3). The record of a broad singlet for the three protons of the rapidly interconverting hexafluoroacetylacetonate anions points to the existence of a dynamically averaged $C_{2v}$-symmetrical $[Ln(hfac)_3(\mathbf{L3^{Ph}})]$ complex (Ln = La, Eu, Y) on the NMR time scale in solution (Figure S4).[25] The lack of solvent or of diglyme molecules bound to the central cation in $[Ln(hfac)_3(\mathbf{L3^{Ph}})]$ (Figure 2) combined with the increasing intensity of the signals of free diglyme monitored by $^1H$ NMR upon titration of $\mathbf{L3^{Ph}}$ with $[Ln(hfac)_3(dig)]$ (Figure S5) are compatible with the ligand exchange reaction depicted in eq 5.

$$[Ln(hfac)_3(dig)] + \mathbf{L3^{Ph}} \rightleftharpoons [Ln(hfac)_3(\mathbf{L3^{Ph}})] + dig$$

$$\beta_{1,1}^{Ln,\mathbf{L3^{Ph}}} = \frac{[Ln(L3^{Ph})]\cdot[dig]}{[Ln]\cdot[\mathbf{L3^{Ph}}]} \quad (5)$$


dx.doi.org/10.1021/ic4030525 | Inorg. Chem. 2014, 53, 3568−3578

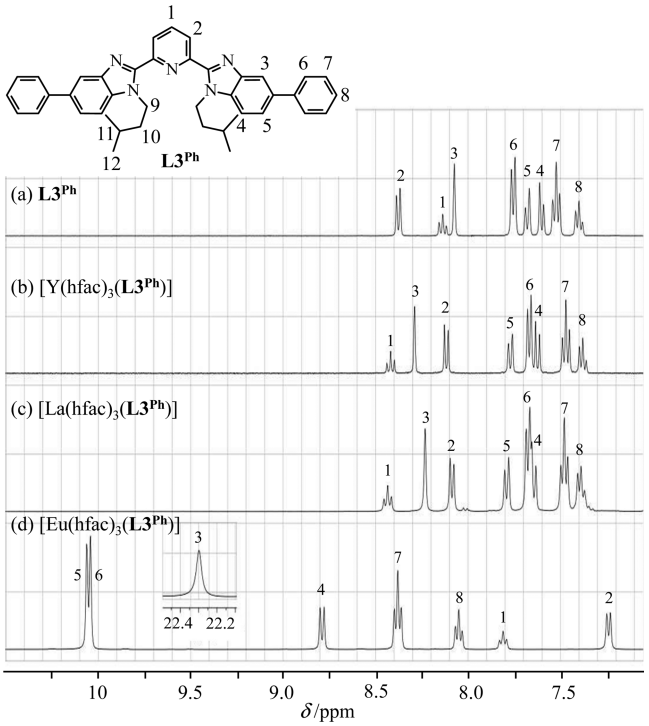


**Figure 3.** Aromatic part with numbering scheme of the $^1$H NMR spectra recorded for (a) $\mathbf{L3^{Ph}}$ and for $[Ln(hfac)_3(\mathbf{L3^{Ph}})]$ (b) Ln = Y, (c) Ln = La, and (d) Ln = Eu in $CD_2Cl_2$ at 293 K and for $[\mathbf{L3^{Ph}}]_{tot}$ = 10 mM. Taking $\beta_{1,1}^{La,dig}$ = 8.3(5)× $10^5$ estimated from Figure S6 and $\beta_{1,1}^{La,\mathbf{L3^{Ph}}}$ = 30, we calculate $K_{diss}^{La(hfac)_3,\mathbf{L3^{Ph}}} = (\beta_{1,1}^{La,\mathbf{L3^{Ph}}}\cdot\beta_{1,1}^{La,dig})^{-1} \simeq 4 \times 10^{-8}$, which results in negligible dissociation for $[La(hfac)_3(\mathbf{L3^{Ph}})]$ at this concentration.

Since (i) the release of the hfac anion from $[Ln(hfac)_3(dig)]$ is minute ($K_{diss}^{Ln,hfac} \leq 10^{-5}$ in aprotic solvents)[25a,27] and (ii) free diglyme cannot be detected for a concentration of $[Ln(hfac)_3(dig)]$ in the $10^{-1}$ to $10^{-5}$ M range in $CD_2Cl_2$ (Ln = Pr, La; Figure S6), we conclude that dissociation of the coligands in $[Ln(hfac)_3(dig)]$ is negligible during NMR titrations performed at 10 mM total ligand concentrations and for occupancy factors $\theta_{Ln} = [Ln]_{bound}/[\mathbf{L}]_{tot}$ in the $0.05 \leq \theta_{Ln} \leq 0.95$ range. The noncomplexed lanthanide metal involved as a reactant in equilibrium 5 therefore exists as the single species $[Ln(hfac)_3(dig)]$ in solution, the concentration of which is written as [Ln] for the rest of this work. Upon the addition of a large excess of diglyme in solution, its concentration can be assumed to be invariant ($[dig] = [dig]_{tot}$), and the equilibrium constant $\beta_{1,1}^{Ln,\mathbf{L3^{Ph}}}$ (eq 5) reduces to its conditional form $\beta_{1,1,cond}^{Ln,\mathbf{L3^{Ph}}}$ (eq 6). The latter parameter is ideally suited for modeling the connection of $Ln(hfac)_3$ to a tridentate $N_3$ binding site to give $[Ln(hfac)_3(\mathbf{L3^{Ph}})]$ in agreement with equilibrium 1, and for which application of eq 2 simply gives $\beta_{1,1,cond}^{Ln,\mathbf{L3^{Ph}}} = f_{N3,cond}^{Ln}$

$$\beta_{1,1,cond}^{Ln,\mathbf{L3^{Ph}}} = \beta_{1,1}^{Ln,\mathbf{L3^{Ph}}}/[dig] = \frac{[Ln(\mathbf{L3^{Ph}})]}{[Ln]\cdot[\mathbf{L3^{Ph}}]} \quad (6)$$

$^1$H NMR titrations of $\mathbf{L3^{Ph}}$ (10 mM) with $[Ln(hfac)_3(dig)]$ (Ln = La, Eu, Y in $CD_2Cl_2$ + 0.14 M diglyme) indeed show the stepwise formation of $[Ln(hfac)_3(\mathbf{L3^{Ph}})]$ as the only product of equilibrium 5 (Figure S7). Integration of the NMR signals of the same proton connected to the free ($I_L$) and complexed ($I_{LnL}$) ligands provides the well-known occupancy factor $\theta_{Ln}$ for each mixture of metal ($[Ln]_{tot}$) and ligand ($[\mathbf{L}]_{tot}$; eq 7, left-hand side), from which the free concentration of metal [Ln] can be easily deduced (eq 7, center and Figure 4).[15,17]

$$\theta_{Ln} = \frac{[Ln]_{bound}}{[\mathbf{L}]_{tot}} = \frac{I_{Ln\mathbf{L}}}{I_{\mathbf{L}} + I_{Ln\mathbf{L}}} = \frac{[Ln]_{tot} - [Ln]}{[\mathbf{L}]_{tot}} = \frac{\beta_{1,1,cond}^{Ln,\mathbf{L}}[Ln]}{1 + \beta_{1,1,cond}^{Ln,\mathbf{L}}[Ln]} \quad (7)$$

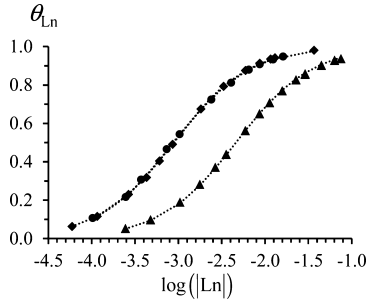


**Figure 4.** Occupancy factors and binding isotherms deduced from $^1$H NMR titration of $\mathbf{L3^{Ph}}$ with $[Ln(hfac)_3(dig)]$ (▲ = La, ● = Eu, ■ = Y) in $CD_2Cl_2$ + 0.14 M dig at 293 K. The dotted lines correspond to the fitted curves computed with eq 7 and using $\beta_{1,1,cond}^{Ln,\mathbf{L}}$ collected in Table 1.

Introduction of the mass balances for ligands and metals together with the law of mass action gives the right-hand side of eq 7, often referred to as the binding polynomial or binding isotherm (see Appendix 1 for details). Nonlinear least-squares fits of the binding isotherms to the experimental occupancy factors (Figure 4) eventually provide the formation constants $\beta_{1,1,cond}^{Ln,\mathbf{L3^{Ph}}}$ and intrinsic affinities $f_{N3,cond}^{Ln}$ collected in Table 1.[28]

**Table 1. Thermodynamic Stability Constants $\beta_{1,1}^{Ln,\mathbf{L3^{Ph}}}$ (eq 5) and $\beta_{1,1,cond}^{Ln,\mathbf{L3^{Ph}}}$ (eq 6) and Intrinsic Affinities $f_{N3,cond}^{Ln}$ and $f_{N3}^{Ln}$ (eq 2)[a] Obtained from the NMR Titrations of $\mathbf{L3^{Ph}}$ with $[Ln(hfac)_3(dig)]$ ($CD_2Cl_2$ + 0.14 M dig; dig = diglyme = 1-Methoxy-2-(2-methoxyethoxy)ethane, 293 K)[28]**

| | $\beta_{1,1}^{Ln,\mathbf{L3^{Ph}}}$ | $f_{N3}^{Ln}$ | $\beta_{1,1,cond}^{Ln,\mathbf{L3^{Ph}}}$ | $f_{N3,cond}^{Ln}$ |
|---|---|---|---|---|
| Ln = La[b] | 30(1) | 30(1) | 217(2) | 217(2) |
| Ln = La[c] | 30(2) | 30(2) | 220(7) | 220(7) |
| Ln = Eu[b] | 149(4) | 149(4) | 1146(13) | 1146(13) |
| Ln = Y[b] | 140(6) | 140(6) | 1129(9) | 1129(9) |

[a]The intrinsic affinity $f_{N3}^{Ln}$ is related to its conditional form by using $f_{N3}^{Ln} = f_{N3,cond}^{Ln}\,[dig]_{tot}$ (eq 6). [b]Computed by integrations of $^1$H NMR signals. [c]Computed by integration of $^{19}$F NMR signals.

The range of stability constants $30 \leq \beta_{1,1}^{Ln,\mathbf{L3^{Ph}}} = \beta_{1,1,cond}^{Ln,\mathbf{L3^{Ph}}}\cdot[dig]_{tot} \leq 50$ deduced from their conditional forms for $[Ln(hfac)_3(\mathbf{L3^{Ph}})]$ ($CD_2Cl_2$, Table 1) are in line with $10 \leq \beta_{1,1}^{Ln,\mathbf{L3^{Br}}} \leq 300$ derived from $\beta_{1,1,cond}^{Ln,\mathbf{L3^{Br}}}$ previously obtained by spectrophotometry in acetonitrile for the analogous complexes $[Ln(hfac)_3(\mathbf{L3^{Br}})]$ (Ln = La–Lu).[25a] The bowl-shape ordering


dx.doi.org/10.1021/ic4030525 | Inorg. Chem. 2014, 53, 3568–3578

of the stability constants $\beta^{La,L3^{Ph}}_{1,1,cond} \ll \beta^{Eu,L3^{Ph}}_{1,1,cond} \geq \beta^{Y,L3^{Ph}}_{1,1,cond}$ along the lanthanide series[1] also mirrors that reported for $L3^{Br}$ in acetonitrile.[25a]

**Synthesis, Characterization, and Thermodynamic Behavior of the Lanthanidopolymers [{Ln(hfac)$_3$}$_m$(L4)].** For solubility reasons, two lipophilic hexyloxy chains were connected to the phenyl spacers in **2**.[29] The target polymer **L4** is then obtained by the Miyaura–Suzuki coupling of $L3^{Br}$ with the diboronic acid **3**, followed by saturation of the terminal reactive bromo and boronic acid sites with inactive phenyl rings (Scheme 3). The $^1$H NMR spectrum of **L4** (Figure 5c) points

**Scheme 3. Synthesis of Polymer L4 Highlighting the Three Planned Possible Termini**

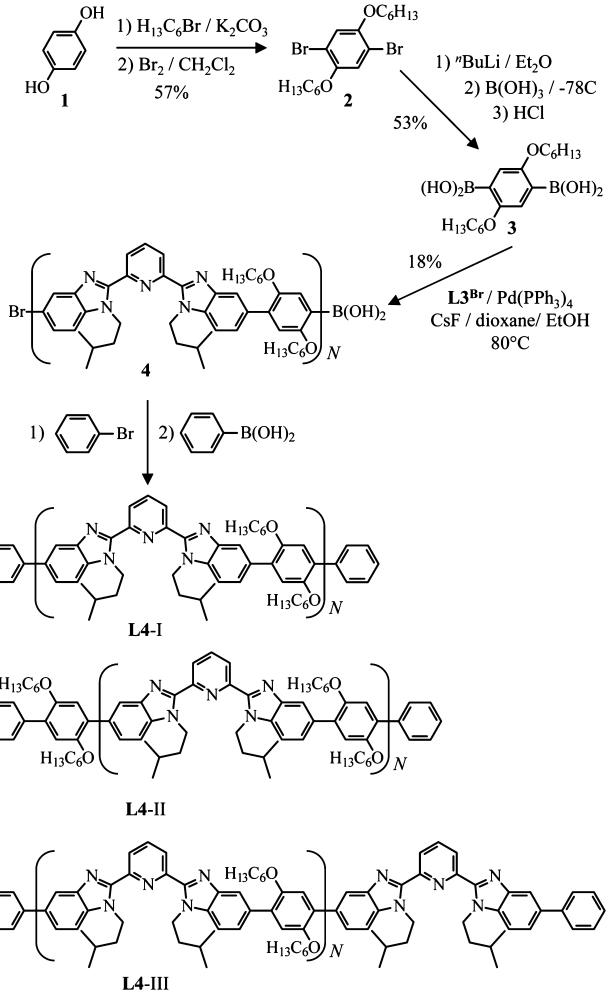


to the expected coexistence of a signals diagnostic for the spacers (H14–H18, Figure 5a) and for the tridentate binding unit (H1–H3, Figure 5b) in a molar ratio close to 1.0, together with a minor amount of signals arising from terminal phenyl rings (H8). The low-resolution ESI mass spectrum of **L4** (Figure S8) shows a large distribution of weak peaks corresponding to fragments with $m/z$ in the range 728 (monomer)–1607 (trimer).

Size extrusion chromatography (SEC) in tetrahydrofuran coupled with a triple-detector (light-scattering, refractive index, light-absorption) indicates a molecular weight distribution of polymers in the 3000–40000 g/mol range (Figure S9) characterized by a number average molecular weight $\bar{M}_n$ =

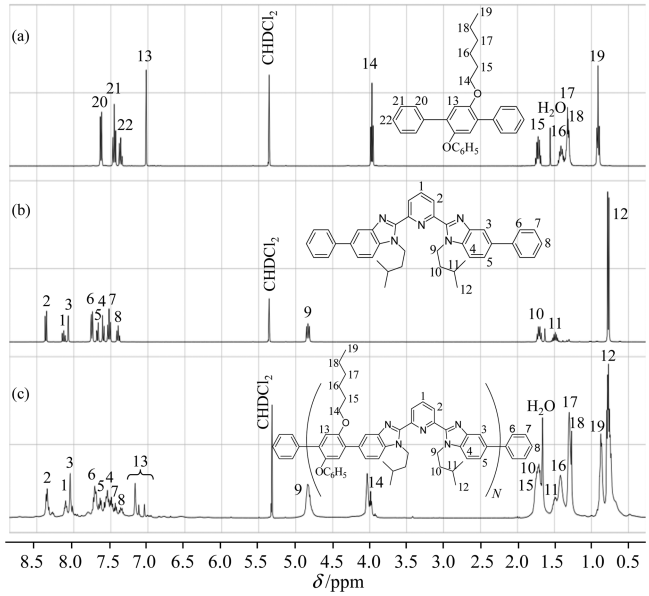


**Figure 5.** $^1$H NMR spectra with assignments and numbering schemes for (a) para-disubstituted 1,4-dihexyloxy-benzene bridge, (b) central tridentate binding unit in $L3^{Ph}$, and (c) polymer **L4**.

5414 g/mol, a weight average molecular weight $\bar{M}_w$ = 7192 g/mol, and a polydispersity index of $I_P = \bar{M}_w/\bar{M}_n$ = 1.33 (see Appendix 3 for details).[30,31]

Because **L4**-I to **L4**-III contribute to **L4** (Scheme 3), an excess of molecular weight ew roughly corresponding to two to five phenyl or benzimidazole groups should be taken into account for the estimation of the average number $\langle N \rangle$ of monomeric units in **L4**, each bringing a molecular mass of $M_0$ = 726 g/mol (eq 8). However, the detection by ESI-MS of a considerable amount of fragments possessing H (reduction) or OH (hydrolysis) termini (Figure S8)[32] lead us to use a more reasonable value of $\overline{ew} \approx 77$ g/mol corresponding to one terminal $C_6H_5$ phenyl unit. We calculate $\langle N \rangle_n$ = 7.4 from the number average molecular weight and $\langle N \rangle_w$ = 9.8 for its counterpart in weight.

$$\langle N \rangle = \frac{\bar{M} - \overline{ew}}{M_0} \tag{8}$$

Titrations of **L4** with [Ln(hfac)$_3$(dig)] (Ln = La, Eu, Y) in $CD_2Cl_2$ + 0.14 M diglyme were monitored by using $^1$H NMR (Figure S10) and $^{19}$F-NMR spectra (Figure 6). The integration of specific signals for protons (H9, Figure S10) belonging to tridentate sites bound to the entering metal ($I^H_{LnL4}$) or free of complexing agent ($I^H_{L4}$) provides the experimental occupancy factors and concentrations of free metal (eq 9, left-hand side) for each $[\mathbf{L4}]_{tot}$:$[Ln]_{tot}$ mixture (Figure 7). The same procedure holds for the integration of signals for fluorine atoms in $^{19}$F NMR spectra (eq 9, right-hand side and Figure 6).


dx.doi.org/10.1021/ic4030525 | Inorg. Chem. 2014, 53, 3568–3578

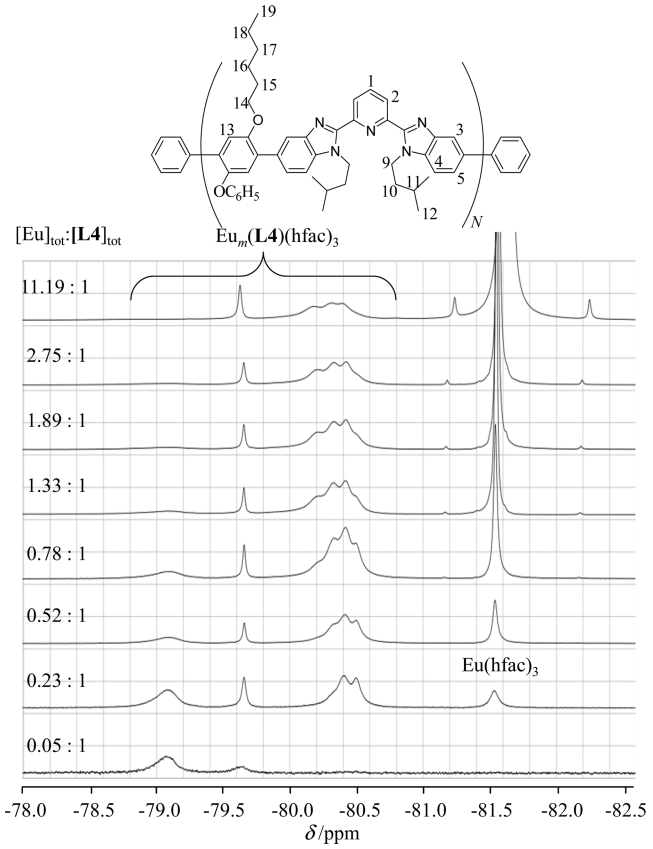


**Figure 6.** $^{19}$F NMR titration of **L4** (3 mM) with [Eu(hfac)$_3$dig] in $CD_2Cl_2$+ 0.14 M dig at 293 K with numbering scheme and assignment.

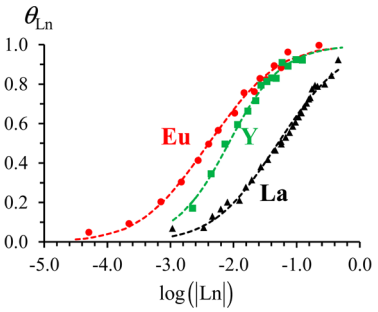


**Figure 7.** Occupancy factors deduced from the $^1$H NMR titrations of **L4** (3 mM) with [Ln(hfac)$_3$dig] (▲ = La (black), ● = Eu (red), and ■ = Y (green)) in $CD_2Cl_2$ + 0.14 M dig at 293 K. The dotted lines correspond to the theoretical binding isotherms fitted with eq 11 for the mixture of oligomers $N$ = 18 (0.16), $N$ = 11 (0.18), $N$ = 9 (0.19), $N$ = 6 (0.25), $N$ = 5 (0.15), $N$ = 4 (0.06), and $N$ = 3 (0.01).

$$\theta_{Ln} = \frac{[Ln]_{bound}}{\langle N\rangle[\mathbf{L4}]_{tot}} = \frac{[Ln]_{tot} - [Ln]}{\langle N\rangle[\mathbf{L4}]_{tot}} = \frac{I^{H}_{Ln\mathbf{L4}}}{I^{H}_{\mathbf{L4}} + I^{H}_{Ln\mathbf{L4}}} = \frac{I^{F}_{Ln\mathbf{L4}}}{I^{F}_{Ln} + I^{F}_{Ln\mathbf{L4}}}\cdot\frac{[Ln]_{tot}}{\langle N\rangle[\mathbf{L4}]_{tot}} \quad (9)$$

A simple approach considers **L4** as a roughly monodisperse polymer containing a single oligomer with an average number $\langle N\rangle_n$ or $\langle N\rangle_w$ of monomeric units. In these conditions, the theoretical modeling of the occupancy factors corresponds to (see Appendix 4 for details):

$$\theta_{Ln} = \frac{[Ln]_{bound}}{\langle N\rangle[\mathbf{L4}^{\langle N\rangle}]_{tot}} = \frac{\sum_{m=0}^{\langle N\rangle} m[Ln_m\mathbf{L4}^{\langle N\rangle}]}{\langle N\rangle\sum_{m=0}^{\langle N\rangle}[Ln_m\mathbf{L4}^{\langle N\rangle}]} = \frac{\sum_{m=0}^{\langle N\rangle} m\beta^{\langle N\rangle}_{m,1}[Ln]^m}{\langle N\rangle\sum_{m=0}^{\langle N\rangle}\beta^{\langle N\rangle}_{m,1}[Ln]^m} \quad (10)$$

where the formation constants $\beta^{\langle N\rangle}_{m,1}$ are obtained with eq 2 using the conditional lanthanide-binding site affinity $f^{Ln}_{i,cond}$ and the intermetallic repulsion $\Delta E^{Ln,Ln}_{1-2}$. Satisfying nonlinear least-squares fits of $\theta_{Ln}$ with eq 10 (agreement factors $0.026 \le AF \le 0.039$)[33] provides a single set of $f^{Ln}_{i,cond}$ and $\Delta E^{Ln,Ln}_{1-2}$ parameters within experimental uncertainties, whatever the choice of the length of the representative oligomer according that $\langle N\rangle > 2$ (Table S7 and Figure S11). A more precise analysis regards **L4** as a mixture of individual receptors of length $N$ occurring at their mole fractions $x_N$, these two characteristics being estimated by a Gaussian deconvolution of the molecular weight distribution of the polymer ($N$ = 18 (0.16), $N$ = 11 (0.18), $N$ = 9 (0.19), $N$ = 6 (0.25), $N$ = 5 (0.15), $N$ = 4 (0.06), and $N$ = 3 (0.01), Figure S12). For a mixture of oligomers, the binding isotherm is modeled with eq 11 where $\theta^N_{Ln}$ are the occupancy factors for each oligomer of length $N$ given in eq 10 (see Appendix 4 for details).

$$\theta_{Ln} = \frac{\sum_{N=1}^{N_{tot}}(x_N N\theta^N_{Ln})}{\sum_{N=1}^{N_{tot}} Nx_N} \quad (11)$$

Repeating the nonlinear least-squares fits of $\theta_{Ln}$ with eq 11 yields the satisfying binding isotherms shown in Figure 7 and built with the help of the conditional lanthanide-binding site affinities $f^{Ln}_{i,cond}$ and the intermetallic interactions $\Delta E^{Ln,Ln}_{1-2}$ gathered in Table 2.

As found for the monomer **L3**$^{Ph}$, the affinities of the lanthanide carriers [Ln(hfac)$_3$] for a tridentate nitrogen binding site in the polymer **L4** display a bowl-shaped dependence with

**Table 2. Thermodynamic Intrinsic Affinities $f^{Ln}_{N3,cond}$ and $f^{Ln}_{N3}$,[a] and Intramolecular Intermetallic Interactions $u^{Ln,Ln}_{1-2} = \exp(-\Delta E^{Ln,Ln}_{1-2}/RT)$ Obtained from the NMR Titrations of Polymer L4 with [Ln(hfac)$_3$(dig)] ($CD_2Cl_2$ + 0.14 M dig; dig = diglyme = 1-Methoxy-2-(2-methoxyethoxy)ethane, 293 K)[b]**

| | $f^{Ln}_{N3}$ | $f^{Ln}_{N3,cond}$ | $u^{Ln,Ln}_{1-2}$ | $\Delta E^{Ln,Ln}_{1-2}$ /kJ·mol$^{-1}$ |
|---|---|---|---|---|
| Ln = La[c,d] | 3.9(2) | 28(1) | 0.66(3) | 1.0(2) |
| Ln = Eu[d] | 56(2) | 397(12) | 0.57(3) | 1.4(2) |
| Ln = Y[c] | 15.5(6) | 111(4) | 1.09(4) | −0.2(1) |

[a]The intrinsic affinity $f^{Ln}_{N3}$ is related to its conditional form by using $f^{Ln}_{N3} = f^{Ln}_{N3,cond}[dig]_{tot}$ (eq 6). [b]**L4** is considered as a mixture of oligomers with $N$ = 18 (0.16), $N$ = 11 (0.18), $N$ = 9 (0.19), $N$ = 6 (0.25), $N$ = 5 (0.15), $N$ = 4 (0.06), and $N$ = 3 (0.01), see text and Figure S12. [c]Computed by integrations of $^1$H NMR signals. [d]Computed by integration of $^{19}$F NMR signals.


dx.doi.org/10.1021/ic4030525 | Inorg. Chem. 2014, 53, 3568−3578

decreasing ionic size ($f^{La}_{N3} < f^{Eu}_{N3} > f^{Y}_{N3}$), a trend similarly found for the intermetallic repulsions ($\Delta E^{La,La}_{1-2} \leq \Delta E^{Eu,Eu}_{1-2} > \Delta E^{Y,Y}_{1-2} \approx 0$). However, the affinity of the binding sites in the polymer are reduced by a factor 3−10 with respect to that measured for the monomer **L3$^{Ph}$**, probably as a result of the increased lipophilicity produced by the long hexyloxy chains connected to the phenyl spacers.[34] Under these conditions, 50% metal loading requires a ratio of $[Ln]_{tot}/[\mathbf{L4}]_{tot}$ = 32 for Ln = La, 7 for Ln = Y, and 6 for Ln = Eu. The minor repulsive (Ln = La, Eu) or negligible (Ln = Y) intramolecular intermetallic interactions are not sufficient to produce a plateau for $\theta_{Ln}$ = 0.5[17b] but nevertheless affect the variances in the number of metals bound to the receptor (Figure S13).

**Photophysical Properties of [Eu(hfac)$_3$(L3$^{Ph}$)] and [{Eu(hfac)$_3$}$_m$(L4)].** The electronic absorption spectra of the tridentate binding site in the monomeric unit **L3$^{Ph}$** is dominated by two broad bands assigned to $\pi^* \leftarrow \pi_1$ (29 670 cm$^{-1}$) and $\pi^* \leftarrow \pi_2$ (38 460 cm$^{-1}$),[35] which are red-shifted by 300−500 cm$^{-1}$ in the polymer **L4** (Figure 8), a trend previously

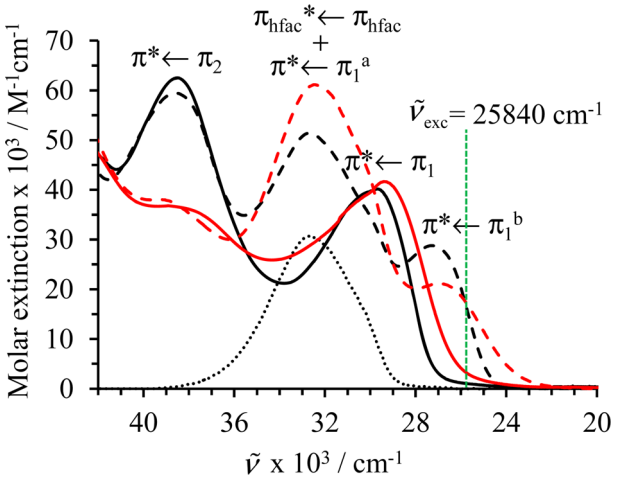


**Figure 8.** Electronic absorption spectra per tridentate binding site recorded for **L3$^{Ph}$** (black full trace), **L4** (red full trace), [Eu(hfac)$_3$(**L3$^{Ph}$**)] (black dashed trace), [{Eu(hfac)$_3$}$_m$(**L4**)] (red dashed trace), and [Eu(hfac)$_3$(dig)] (black dotted trace) in $CH_2Cl_2$ + $10^{-4}$ M diglyme at 293 K. The absorption spectra were recorded for $[Eu]_{tot}$ = 7 × $10^{-5}$ M and corrected for partial dissociation in solution (see Appendix 5). The vertical dotted green trace indicates the exitation energy used for recording the emission spectra of the complexes.

documented when two alkoxy groups were connected to the phenyl bridge of ligand **L5** to give **L6** (Scheme 4).[24b] Upon coordination to trivalent europium in [Eu(hfac)$_3$(**L3$^{Ph}$**)] and [{Eu(hfac)$_3$}$_m$(**L4**)], the $\pi^* \leftarrow \pi_1$ transition is split by the complexation process,[36] the low-energy component $\pi^* \leftarrow \pi_1^b$ at 26 500 cm$^{-1}$ being exploited for the selective excitation of the

**Scheme 4. Chemical Structures of Ligands L5−L7[24b]**

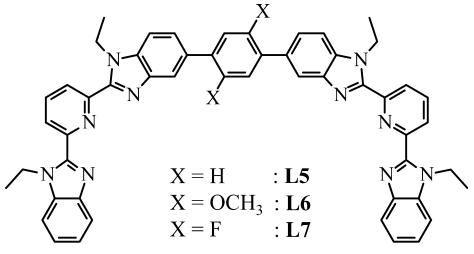


coordinated tridentate site with minor perturbations due to competitive light absorption by the free ligand or by the free metal [Eu(hfac)$_3$(dig)] (Figure 8).

Excitation of the tridentate coordinated sites at $\tilde{\nu}_{exc}$ = 25 840 cm$^{-1}$ in [Eu(hfac)$_3$(**L3$^{Ph}$**)] and [{Eu(hfac)$_3$}$_m$(**L4**)] (Figure 8) produces residual ligand-centered emission ($^1\pi^* \rightarrow {}^1\pi + {}^3\pi^* \rightarrow {}^1\pi$, Figure S14) together with an intense red luminescence arising from **Lk** → Eu energy transfer followed by Eu($^5D_1$)- and Eu($^5D_0$)-centered phosphorescence (Figure 9). The intensities

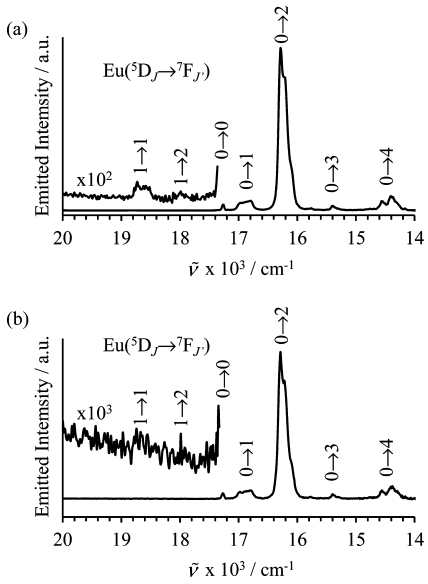


**Figure 9.** Emission spectra recorded for (a) [Eu(hfac)$_3$(**L3$^{Ph}$**)] ($10^{-5}$ M, $\theta_{Eu}$ = 0.98) and (b) [{Eu(hfac)$_3$}$_m$(**L4**)] (6 × $10^{-6}$ M, $\theta_{Eu}$ = 0.85) in $CH_2Cl_2$ + $10^{-4}$ M diglyme at 293 K upon excitation at $\tilde{\nu}_{exc}$ = 25 840 cm$^{-1}$.

of the Eu($^5D_1 \rightarrow {}^7F_J$) transitions are extremely small compared with the luminescence arising from the Eu($^5D_0 \rightarrow {}^7F_J$) transitions, and the emission spectra are dominated by the hypersensitive forced electric dipolar Eu($^5D_0 \rightarrow {}^7F_2$) transition centered at 16 240 cm$^{-1}$. These two spectral characteristics are diagnostic for low-symmetry tris-$\beta$-diketonate Eu(III) complexes.[24,25] The experimental absolute quantum yield $\Phi^L_{Eu}$ (determined upon excitation of the ligand and monitoring the $Eu^{3+}$ emission in dichloromethane solution) reaches 45(1)% for [Eu(hfac)$_3$(**L3$^{Ph}$**)] in line with the 35% reported for [Eu(hfac)$_3$(diglyme)] in ether/isopentane/ethanol (5:5:2)[37a] and with 40% ≤ $\Phi^L_{Eu}$ ≤ 60% reported for optimized [Eu(**L**)($\beta$-diketonate)$_3$] complexes where **L** are chelating N-donor or O-donor ligands and $\beta$-diketonate stands for the hexafluoroacacetylacetonate or for unsymmetrical 2-thienoyltrifluoroacetonate.[37b−g] The quantum yield reduces to $\Phi^L_{Eu}$ = 0.41(3) % for the occupied tridentate binding sites in [{Eu(hfac)$_3$}$_m$(**L4**)] ($\theta_{Eu}$ = 0.85, Table 3), a value much smaller than the quantum yields determined for the relevant dinuclear complexes [{Eu(hfac)$_3$}$_2$(**L5**)] ($\Phi^L_{Eu}$ = 9.3(3)%) and [{Eu(hfac)$_3$}$_2$(**L6**)] ($\Phi^L_{Eu}$ = 9.2(3)%) in the solid state.[24b] Our procedure for correcting light absorption for partial dissociation occurring in solution (see Appendix 5 for details) is validated by closely related results obtained at variable occupancy factors (Table 3). The observed minor variation 0.25% ≤ $\Phi^L_{Eu}$ ≤ 0.41% is attributed to the different electronic structures resulting from the increasing occupancy of adjacent binding sites upon metal


dx.doi.org/10.1021/ic4030525 | Inorg. Chem. 2014, 53, 3568−3578

Table 3. Absolute Quantum Yields $\Phi_{Eu}^{L}$ Obtained for the Occupied Tridentate Binding Sites in $[Eu(hfac)_3(L3^{Ph})]$ and $[\{Eu(hfac)_3\}_m(L4)]$ in $CH_2Cl_2$ + $10^{-4}$ M dig at 293 K

| | $\theta_{Eu}$[a] | $\tilde{\nu}_{exc}/cm^{-1}$ | $\Phi_{Eu}^{L}/\%$[b] |
|---|---|---|---|
| $[Eu(hfac)_3(L3^{Ph})]$ | 0.98 | 25840 | 45(1) |
| $[\{Eu(hfac)_3\}_m(L4)]$ | 0.30 | 25840 | 0.25(1) |
| $[\{Eu(hfac)_3\}_m(L4)]$ | 0.59 | 25840 | 0.27(2) |
| $[\{Eu(hfac)_3\}_m(L4)]$ | 0.85 | 25840 | 0.41(3) |

[a]Occupancy factor computed for the complex in solution. [b]Upon irradiation at $\tilde{\nu}_{exc}$ = 25 840 $cm^{-1}$, $[Eu(hfac)_3(dig)]$ did not luminesce, and the quantum yield was therefore only corrected for changes in absorption resulting from partial dissociation at $[L]_{tot} = 6 \times 10^{-5}$ M (see Appendix 5 for details).

loading, a phenomenon substantiated by the record of slightly different absorption spectra (Figure S15).

Since the light-harvesting properties are comparable in the monomer **L3$^{Ph}$** and in the polymer **L4**, we conclude that the drastic decrease by 2 orders of magnitude of the global quantum yields of the Eu-bound sites in $[\{Eu(hfac)_3\}_m(L4)]$ results from nonradiative loss following light absorption. The connection of alkyloxy groups to the phenyl bridges is known to reduce the efficiency of the ligand-centered ($^3\pi^*$) → Eu($^5D_{1,0}$) energy transfer processes by a factor of 2 in the dinuclear complexes with **L6**,[24b] but further pertinent rationalization requires the decipherment of each step of the energy migration process in the polymer (intersystem crossing, ligand-to-Eu energy transfer, and intrinsic Eu(III) quantum yield).[24b]

## EXPERIMENTAL SECTION

Chemicals were purchased from Strem, Acros, Fluka AG, and Aldrich and used without further purification unless otherwise stated. The ligand **L3$^{Br}$** was synthesized according to a literature procedure.[25a] The hexafluoroacetylacetonate salts $[Ln(hfac)_3(dig)]$ were prepared from the corresponding oxide (Aldrich, 99.99%).[26] Acetonitrile and dichloromethane were distilled over calcium hydride. Silica gel plates Merck 60 $F_{254}$ were used for thin layer chromatography (TLC) and Fluka silica gel 60 (0.04−0.063 mm), or Acros neutral activated alumina (0.050−0.200 mm) was used for preparative column chromatography.

**Preparation of Phenylboronic Acid.** *n*-Butyllithium (20.86 mL, 1.6 M in hexane, 33.4 mmol) was added dropwise to a solution of bromobenzene (5.0 g, 31.8 mmol) in dry THF (10 mL) at −78 °C. The reaction mixture was stirred under an inert atmosphere at −78 °C for 45 h; then trimethylborate (1.7 mL, 15 mmol) was added dropwise, and the resulting solution was stirred for one night at RT. Aqueous hydrochloric acid (2 M, 40 mL) was added and the mixture stirred for 1 h. Tetrahydrofuran was evaporated, and the crude product was extracted with diethyl ether (3 × 100 mL). The combined organic layers were dried over anhydrous $Na_2SO_4$, filtered, and evaporated to dryness. The residue was purified by crystallization in heptane to give phenylboronic acid (1.3 g, 10.7 mmol, yield: 33%) as a white powder. $^1$H NMR ($CDCl_3$; 400 MHz), $\delta$/ppm: 7.54 (dt, $^3J$ = 6.9 Hz, $^4J$ = 1.3 Hz, 2H), 7.63 (dt, $^3J$ = 7.2 Hz, $^4J$ = 1.2 Hz, 1H), 8.28 (dd, $^3J$ = 6.9 Hz, $^4J$ = 1.2 Hz, 2H). ESI-MS ($CH_2Cl_2$, negative mode): $m/z$ 121.1 ($[M - H]^-$).

**Preparation of 1,4-Dihexyloxybenzene.** A mixture of hydroquinone (**1**, 5.5 g, 49.7 mmol), 1-bromohexane (16 mL, 114 mmol), and $K_2CO_3$ (25 g, 181 mmol) in dry acetone (150 mL) was refluxed for 3 days. The solvent was removed, and the crude product was dissolved in diethyl ether (200 mL) and washed with water (3 × 80 mL). The organic layer was dried over anhydrous $Na_2SO_4$, filtered, and evaporated to dryness. Crystallization of the crude product in methanol gave 1,4-dihexyloxybenzene (8.05 g, 29 mmol, yield: 57.7%) as a white powder. $^1$H NMR ($CDCl_3$; 400 MHz), $\delta$/ppm: 0.93 (t, $^3J$ = 7.0 Hz, 6H), 1.33−1.39 (m, 8H), 1.47−1.53 (m, 4H), 1.77−1.85 (m, 4H), 3.92 (t, $^3J$ = 6.6 Hz, 4H), 6.84 (s, 4H). ESI-MS ($CH_2Cl_2$): $m/z$ 279.1 ($[M + H]^+$), 296.3 ($[M + NH_4]^+$), 574 ($[2M + NH_4]^+$).

**Preparation of 2,5-Dihexyloxy-1,4-dibromobenzene (2).** Bromine (1.7 mL, 30 mol) in dry $CH_2Cl_2$ (7 mL) was added dropwise to a solution of 1,4-dihexyloxybenzene (3.05 g, 11 mol) in dry $CH_2Cl_2$ (30 mL) at 0 °C. The reaction mixture was stirred at room temperature for 12 h. Dichloromethane (100 mL) was then added, and the organic layer was successively washed with water (2 × 50 mL) and with aqueous $Na_2S_2O_4$ (2 M, 2 × 50 mL), then dried over anhydrous $Na_2SO_4$, filtered, and evaporated to dryness. The residue was purified by crystallization in ethanol to give 2,5-dihexyloxy-1,4-dibromobenzene (**2**, 4.35 g, 10.7 mmol, yield: 91.9%) as a white powder. $^1$H NMR ($CDCl_3$; 400 MHz), $\delta$/ppm: 0.93 (t, $^3J$ = 7.0 Hz, 6H), 1.34−1.39 (m, 8H), 1.47−1.53 (m, 4H), 1.77−1.85 (m, 4H), 3.97 (t, $^3J$ = 6.5 Hz, 4H), 7.10 (s, 2H). ESI-MS ($CH_2Cl_2$): $m/z$ 454 ($[M + H_3O]^+$).

**Preparation of 2,5-Dihexyloxy-1,4-phenylenediboronic Acid (3).** *n*-Butyllithium (7.8 mL, 1.6 M in hexane, 12.5 mmol) was added dropwise to a solution of **2** (2.2 g, 5 mmol) in dry diethylether (50 mL) at 0 °C. The reaction mixture was stirred at room temperature under an inert atmosphere for 7 h, then cooled to −78 °C. Trimethylborate (1.7 mL, 15 mmol) was added dropwise, and the solution was stirred for 12 h at RT. Aqueous hydrochloric acid (2m, 40 mL) was added and stirred for 2 h. Diethyl ether was evaporated, and the resulting solid was filtered and washed with diethyl ether and ethyl acetate. Removal of the volatile solvents under a vacuum gave 2,5-dihexyloxy-1,4-diboronic acid (**3**, 0.97 g, 2.65 mmol, yield: 53%) as a white powder. $^1$H NMR ($CDCl_3$; 400 MHz), $\delta$/ppm: 0.88 (t, $^3J$ = 7.0 Hz, 6H), 1.29−1.36 (m, 8H), 1.38−1.46 (m, 4H), 1.69−1.76 (m, 4H), 3.99 (t, $^3J$ = 6.4 Hz, 4H), 7.18 (s, 2H), 7.80 (s, 4H, OH). ESI-MS ($CH_2Cl_2$, negative mode): $m/z$ 365.1 ($[M - H]^-$).

**Preparation of 2,6-Bis-[1-(3-methylbutyl)-5-phenyl-benzimidazol-2-yl]pyridine (L3$^{Ph}$).** 2,6-Bis-[1-(3-methylbutyl)-5-bromo-benzimidazol-2-yl]pyridine (**L3$^{Br}$**, 597 mg, 0.98 mmol), phenylboronic acid (300 mg, 2.46 mmol), $K_2CO_3$ (677 mg, 4.90 mmol), and tetrakis(triphenylphosphine)palladium (113 mg, 0.098 mmol) were loaded into a Schlenk tube, which was flushed with argon. A degassed mixture of dioxane (10 mL) and ethanol (6 mL) was added, and the resulting solution was stirred at 80 °C for 24 h. Aqueous half-saturated $Na_2CO_3$ was added (20 mL), and the mixture was extracted with dichloromethane (3 × 50 mL). The combined organic phases were washed with brine, dried over anhydrous $Na_2SO_4$, filtered, and evaporated to dryness. The crude product was purified by flash column chromatography (Silicagel; hexane/ethylacetate = 1:1) to give **L3$^{Ph}$** as a white solid (484 mg, 0.80 mmol, yield: 82%). $^1$H NMR (400 MHz, $CDCl_3$): $\delta$ 8.36 (d, $^3J$ = 7.9 Hz, 2H), 8.11 (d, $^2J$ = 1.2 Hz, 1H), 8.10 (t, $^3J$ = 7.9 Hz, 2H), 7.72 (d, $^3J$ = 7.1 Hz, 4H), 7.65 (dd, $^3J$ = 8.4, $^4J$ = 1.6 Hz, 2H), 7.54 (d, $^3J$ = 8.5 Hz, 2H), 7.50 (t, $^3J$ = 7.7 Hz, 4H), 7.38 (t, $^3J$ = 7.4 Hz, 2H), 4.77 (t, $^3J$ = 7.6 Hz, 4H), 1.68 (q, $^3J$ = 7.1 Hz, 4H), 1.45 (sept, $^3J$ = 6.6 Hz, 2H), 0.75 (d, $^3J$ = 6.6 Hz, 12H). $^{13}$C NMR (101 MHz, $CDCl_3$): $\delta$ 150.95 (2 $C_{quat}$), 150.16 (2 $C_{quat}$), 143.64 (2 $C_{quat}$), 141.94 (2 $C_{quat}$), 138.49 (CH), 136.68 (2 $C_{quat}$), 135.95 (2 $C_{quat}$), 129.07 (4 CH), 127.66 (4 CH), 127.12 (2 CH), 125.76 (2 CH), 123.62 (2 CH), 118.90 (2 CH), 110.63 (2 CH), 43.84 (2 $CH_2$), 39.11 (2 $CH_2$), 26.03 (2 CH), 22.44 (4 $CH_3$). ESI-MS ($CH_3OH$): $m/z$ 604.5 ($[L3^{Ph} + H]^+$).

**Preparation of Polymer (L4).** 2,6-Bis-[1-(3-methylbutyl)-5-bromo-benzimidazol-2-yl]pyridine (**L3$^{Br}$**, 1.000 g, 1.64 mmol), 2,5-dihexyloxy-1,4-diboronic acid (**3**, 599.9 mg, 1.64 mmol), and CsF (1.493 mg, 9.83 mmol, 6 equiv) were dissolved in dry dioxane (40 mL). The solution was degassed with argon for 30 min before adding $Pd(PPh_3)_4$ (190.1 mg, 0.165 mmol, 10% equiv). The reaction mixture was further degassed for 30 min, then stirred under argon at 80 °C for 3 days. The polymerization was completed with the addition of bromobenzene (259.12 mg, 1.64 mmol, 1 equiv) and $Pd(PPh_3)_4$ (25 mg), followed 24 h later with the addition of phenylboronic acid (201.72 mg, 1.64 mmol, 1 equiv). The final mixture was stirred for 24 h at RT, and the solvents were removed. The residue was dissolved in chloroform (300 mL) and the organic phase successively washed with brine (3 × 90 mL) and water (150 mL). The organic layer was dried


dx.doi.org/10.1021/ic4030525 | Inorg. Chem. 2014, 53, 3568−3578

($Na_2SO_4$), filtered, and evaporated to dryness. The solid was dissolved in a minimum amount of chloroform, then poured dropwise into methanol (450 mL). Centrifugation provided a sediment, which was dispersed in methanol (50 mL). A second centrifugation gave a solid residue, which was dried under a vacuum, redissolved in a minimum amount of chloroform and poured into heptane (400 mL). Centrifugation followed by decantation and drying gave **L4** (215 mg, 18%) as a pale brown solid. This fractionation process can be repeated to reduce the polydispersity index at the cost of the total yield.

**Preparation of the Complexes [Ln(hfac)$_3$(L3$^{Ph}$)] (Ln = La, Eu, Y).** Stoichiometric amounts of **L3$^{Ph}$** and [Ln(hfac)$_3$(dig)] were reacted in acetonitrile/chloroform (1.00:0.12 mL). Slow evaporation provided X-ray quality crystals of [Ln(hfac)$_3$(**L3$^{Ph}$**)] in 40−60% yields.

*[La(hfac)$_3$(**L3$^{Ph}$**)].* $^1$H NMR (400 MHz, $CD_2Cl_2$): $\delta$ 8.43 (t, $^3J$ = 7.9 Hz, 1H), 8.23 (s, 2H), 8.09 (d, $^3J$ = 8.0 Hz, 2H), 7.79 (d, $^3J$ = 8.6 Hz, 2H), 7.68 (d, $^3J$ = 7.8 Hz, 4H), 7.64 (d, $^3J$ = 8.9 Hz, 2H), 7.48 (t, $^3J$ = 7.4 Hz, 4H), 7.39 (t, $^3J$ = 7.3 Hz, 2H), 5.89 (s, 3H), 4.62 (t, $^3J$ = 8.4 Hz, 4H), 2.03 (dt, $^3J$ = 12.0 Hz, 6.8 Hz, 4H), 1.91 (dq, $^3J$ = 12.9, 6.7 Hz, 2H), 1.13 (d, $^3J$ = 6.5 Hz, 12H). Elem. analyses calcd for $C_{56}H_{44}F_{18}LaN_5O_6$: C, 49.32; H, 3.25; N, 5.14. Found: C, 49.37; H, 3.14; N, 5.15.

*[Eu(hfac)$_3$(**L3$^{Ph}$**)].* $^1$H NMR (400 MHz, $CD_2Cl_2$): $\delta$ 22.30 (s, 2H), 10.05 (d, $^3J$ = 8.0 Hz, 6H), 8.79 (d, $^3J$ = 8.5 Hz, 2H), 8.38 (t, $^3J$ = 7.4 Hz, 4H), 8.05 (t, $^3J$ = 7.3 Hz, 2H), 7.81 (t, $^3J$ = 7.6 Hz, 1H), 7.24 (d, $^3J$ = 7.7 Hz, 2H), 6.02 (t, $^3J$ = 8.0 Hz, 4H), 3.13 (dt, $^3J$ = 11.4, 6.9 Hz, 4H), 2.46 (dq, $^3J$ = 12.9, 6.4 Hz, 2H), 2.34 (br s, 3H), 1.45 (d, $^3J$ = 6.5 Hz, 12H). Elem. analyses calcd for $C_{56}H_{44}EuF_{18}N_5O_6$: C, 48.85; H, 3.22; N, 5.09. Found: C, 48.77; H, 3.19; N, 4.99.

*[Y(hfac)$_3$(**L3$^{Ph}$**)].* $^1$H NMR (400 MHz, $CD_2Cl_2$): $\delta$ 8.42 (t, $^3J$ = 8.0 Hz, 1H), 8.29 (s, 2H), 8.12 (d, $^3J$ = 8.1 Hz, 2H), 7.77 (d, $^3J$ = 8.6 Hz, 2H), 7.67 (d, $^3J$ = 7.6 Hz, 4H), 7.62 (d, $^3J$ = 8.6 Hz, 2H), 7.47 (t, $^3J$ = 7.6 Hz, 4H), 7.38 (t, $^3J$ = 7.4 Hz, 2H), 5.89 (s, 3H), 4.65 (t, $^3J$ = 8.3 Hz, 4H), 2.05 (dt, $^3J$ = 12.3, 7.0 Hz, 4H), 1.96 (dq, $^3J$ = 13.1, 6.5 Hz, 2H), 1.17 (d, $^3J$ = 6.5 Hz, 12H). Elem. analyses calcd for $C_{56}H_{44}F_{18}N_5O_6Y$: C, 51.19; H, 3.38; N, 5.33. Found: C, 50.96; H, 3.30; N, 5.22.

**Spectroscopic and Analytic Measurements.** $^1$H, $^{19}$F, and $^{13}$C NMR spectra were recorded at 293 K on Bruker Avance 400 MHz and Bruker DRX-300 MHz spectrometers. Chemical shifts are given in parts per million with respect to tetramethylsilane $Si(CH_3)_4$. Pneumatically assisted electrospray (ESI) mass spectra were recorded from $10^{-4}$ M solutions on an Applied Biosystems API 150EX LC/MS System equipped with a Turbo Ionspray source. Elemental analyses were performed by K. L. Buchwalder from the Microchemical Laboratory of the University of Geneva. Electronic absorption spectra in the UV−vis were recorded at 20 °C from solutions in $CH_2Cl_2$ with a Perkin-Elmer Lambda 900 spectrometer using quartz cells of 10 or 1 mm path length. Emission spectra were measured using a Jobin Yvon−Horiba Fluorolog-3 spectrofluorimeter. Spectra were corrected for both excitation and emission responses (excitation lamp, detector, and both excitation and emission monochromator responses). Quartz tube sample holders were employed. The quantum yields $\Phi$ in solution were determined through the relative method with respect to quinine sulfate $6.42 \times 10^{-6}$ M in 0.05 M $H_2SO_4$ (refractive index 1.338 and quantum yield 0.546)[38] and to europium-tris(dipoclinate) $6.87 \times 10^{-5}$ M in aqueous tris-buffer (quantum yield 0.24(2)),[39] and using the equation

$$\frac{\Phi_x}{\Phi_r} = \frac{A_r(\bar{\nu})I_r(\bar{\nu})n_x^2D_x}{A_r(\bar{\nu})I_r(\bar{\nu})n_x^2D_x}$$

where $x$ refers to the sample and r to the reference; $A$ is the absorbance corrected for partial dissociation in solution (see Appendix 5), $\nu$ is the excitation wavenumber used, $I$ is the intensity of the excitation light at this energy, $n$ is the refractive index, and $D$ is the integrated emitted intensity. Size extrusion chromatogramms (SEC) were obtained in THF at 30 °C at a rate of 1 mL/min by using a Viscotek GPC max with a VE2001 module (calibrated for molecular mass in the range 1.5−40 kD) coupled with a triple-detection array 305.

**X-Ray Crystallography.** Summary of crystal data, intensity measurements, and structure refinements for [La(hfac)$_3$(**L3$^{Ph}$**)]·0.34$CH_3CN$ are collected in Table S1 (Supporting Information). The crystal was mounted on a quartz fiber with protection oil. Cell dimensions and intensities were measured at 180 K on an Agilent Supernova diffractometer with mirror-monochromated Cu[K$\alpha$] radiation ($\lambda$ = 1.54187). Data were corrected for Lorentz and polarization effects and for absorption. The structure was solved by direct methods (SIR97);[40] all other calculations were performed with ShelX97[41] systems and ORTEP[42] programs. The terminal $CF_3$ groups of the hfac ligands were disordered by rotation about the C(carbonyl)−C($F_3$) axis. Two $CF_3$ groups were refined with two different positions for the fluorine atoms (occupancy factor 0.5), and with isotropic displacement parameters. The 3-methyl-butyl substituent C38−C41 was also disordered and refined using two positions for each carbon atom (occupancy factor 0.5). These carbon atoms were refined isotropically. The acetonitrile molecule lied close to the disordered C38−C41 alkyl residue with an occupancy factor of 0.34. CCDC-964625 contains the supplementary crystallographic data. The cif files can be obtained free of charge via www.ccdc.cam.ac.uk/conts/retrieving.html (or from the Cambridge Crystallographic Data Centre, 12 Union Road, Cambridge CB2 1EZ, U. K.; fax: (+ 44) 1223−336−033 or deposit@ccdc.cam.ac.uk).

## ■ CONCLUSION

The Miyaura−Suzuki procedure used for alternating tridentate bis-benzimidazole pyridine binding units with 1-4-phenyl spacers produces either monodisperse monomer **L3$^{Ph}$** or polymers **L4** constituted of oligomers with variable lengths ($N$ = 3−18 repetitive units), the polydispersity of which can be tuned by successive fractionations. For imperative solubility reasons, the phenyl bridges in the polymers are decorated with lipophilic hexyloxy chains, which proved to have a strong influence on the metal-binding properties. Application of statistical mechanics provides a comprehensive thermodynamic picture of the metal loading process occurring in the Wolf type-II lanthanidopolymers [{Ln(hfac)$_3$}$_m$(**L4**)] in dichloromethane. Compared to the monomer, the affinity of the tridentate binding site in the polymer is reduced by a factor 3−10, an issue tentatively assigned to solvation effects resulting from the increased lipophilicity of the receptor. On the contrary, the bowl-shaped trend of the stability constants along the lanthanide series is amplified in the polymer showing a pronounced maximum around Ln = Eu. Though weak, the observed intramolecular intermetallic interactions are unambiguously repulsive (i.e., anticooperative) for the larger cations, which contributes to stabilizing a special microstate with $\theta_{Ln}$ = 0.5 (strict alternation of occupied and empty sites).[15] However, the magnitudes of $\Delta E_{1-2}^{La,La}$ or $\Delta E_{1-2}^{Eu,Eu}$ are too small to produce the double-hamped distribution of sites required for the isolation of the planned organized half-filled metallopolymer (Figure S13). The accurate speciation of the lanthanidopolymers in solution is used to safely address the electronic absorption and emission properties of the empty and of the occupied tridentate binding sites. As found for thermodynamic metal ligand affinities, the connection of hexyloxy chains to the phenyl spacer also drastically affects the photophysical properties, especially the global quantum yield, which is reduced by 2 orders of magnitude. Additional investigations are required for a definitive assignment of its electronic, solvation, and/or conformational origin, but we note that the connection of electron-withdrawing groups produces the opposite effects, leading to an increase of the quantum yield


dx.doi.org/10.1021/ic4030525 | Inorg. Chem. 2014, 53, 3568−3578

with ligand **L7** (Scheme 4).[24] The design of new lipophilic phenyl bridges following this strategy would therefore be highly welcome for improving polymer luminescence. Finally, the ultimate goal of producing a strict alternation of binding sites occupied by two different lanthanides in a linear polymer requires that $\Delta E_{mix}^{Ln1,Ln2} = (\Delta E_{1-2}^{Ln1,Ln1} + \Delta E_{1-2}^{Ln2,Ln2})/2 - \Delta E_{1-2}^{Ln1,Ln2} > 0$, where $\Delta E_{mix}^{Ln1,Ln2}$ is the mixing intermetallic interaction.[16b] The latter condition is thought to be privileged for systems displaying variable homometallic intersite interactions $\Delta E_{1-2}^{Ln1,Ln1}$,[21,19] a trend maximized in going from Ln = Eu to Ln = Y for the investigated lanthanidopolymers [{Ln(hfac)$_3$}$_m$(**L4**)] (Ln = La, Eu, Y).

## ■ ASSOCIATED CONTENT

### Supporting Information

Details for the determination of occupancy factors and binding isotherms (appendices 1 and 4), for the analysis of the crystal structure of [La(hfac)$_3$(**L3$^{Ph}$**)] (appendix 2), for the calculations of molecular weight distributions (appendix 3), and for the correction of electronic absorption spectra (appendix 5). Tables of crystal data, geometric parameters, bond valences, and thermodynamic descriptors. Figures showing molecular structures, $^1$H NMR spectra and titrations, ESI mass spectra, SEC chromatogramms, binding isotherms, electronic absorption, and emission spectra. A CIF file for [La(hfac)$_3$(**L3$^{Ph}$**)]. This material is available free of charge *via* the Internet at http://pubs.acs.org.

## ■ AUTHOR INFORMATION


### Corresponding Author

*E-mail: Claude.Piguet@unige.ch.

### Author Contributions

[§]The first two authors contributed equally to this research work.


### Notes

The authors declare no competing financial interest.

## ■ ACKNOWLEDGMENTS

Financial support from the Swiss National Science Foundation is gratefully acknowledged.

## ■ REFERENCES


(1) The current IUPAC recommendation is that the name lanthanoid be used rather than lanthanide for the series of elements from La (Z = 57) to Lu (Z = 71), because the suffix "-oid" indicates similarity to one of the members of the containing family of elements. Therefore, Y(III) (Z = 39) does not explicitly belong to the lanthanoid series, but its close similarity to Ho(III) in terms of size and complexation behavior justifies its incorporation as a member of the series. The term rare earth applies for the global consideration of the lanthanoid series combined with Y (Z = 39) and Sc (Z = 21). However, the name lanthanide is still favored in most scientific articles, and for the sake of clarity and simplicity, it is used in this work as a general statement for the lanthanoid series incorporating Y.

(2) (a) Eliseeva, S. V.; Bünzli, J.-C. G. *New J. Chem.* **2011**, *35*, 1165−1176. (b) Bünzli, J.-C. G. *Kirk-Othmer Encyclopedia of Chemical Engineering*; John Wiley & Sons Ed.: New York, 2013; DOI: 10.1002/0471238961.1201142019010215.a01.pub3.

(3) (a) Molander, G. A. *Chem. Rev.* **1992**, *92*, 29−68. (b) Steel, P. G. *J. Chem. Soc., Perkin Trans. 1* **2001**, 2727−2751.

(4) (a) Jüstel, T.; Nikol, H.; Ronda, C. *Angew. Chem., Int. Ed.* **1998**, *37*, 3084−3103. (b) Ronda, C. *J. Luminesc.* **2002**, *100*, 301−305. (c) Auzel, F. *Chem. Rev.* **2004**, *104*, 139−173. (d) van der Ende, B. M.; Aarts, L.; Meijerink, A. *Phys. Chem. Chem. Phys.* **2009**, *11*, 11081−11095. (e) Huang, X.; Han, S.; Huang, W.; Liu, X. *Chem. Soc. Rev.* **2013**, *42*, 173−201.

(5) Cheng, Y. P.; Waters, K. E. *Miner. Eng.* **2013**, *41*, 97−114.

(6) Dos-Santos-Garcia, A. J.; Alario-Franco, M. A.; Saez-Puche, R. *Rare Earth Elem.* **2012**, 371−384.

(7) Thompson, L. C. *Handbook on the Physics and Chemistry of Rare Earth*; Gschneidner, K. A. J., Eyring, L., Eds.; North Holland Publish. Co.: Amsterdam, 1979; chapter 25, pp 209−298.

(8) (a) Pandya, S.; Yu, J.; Parker, D. *Dalton Trans.* **2006**, 2757−2766. (b) Eliseeva, S. V.; Bünzli, J.-C. G. *Chem. Soc. Rev.* **2010**, *39*, 189−227. (c) Carr, R.; Evans, N. H.; Parker, D. *Chem. Soc. Rev.* **2012**, 7673−7686. (d) Thielemann, D. T.; Wagner, A. T.; Rösch, E.; Kölmel, D. K.; Heck, J. G.; Rudat, B.; Neumaier, M.; Feldmann, C.; Scheppers, U.; Bräse, S.; Roesky, P. W. *J. Am. Chem. Soc.* **2013**, *135*, 7454−7457. (e) See also http://www.lumiphore.com/ for recent high-tech developments.

(9) (a) Caravan, P. *Chem. Soc. Rev.* **2006**, *35*, 512−523. (b) Bottrill, M.; Kwok, L.; Long, N. J. *Chem. Soc. Rev.* **2006**, *35*, 557−571. (c) Terreno, E.; Delli Castelli, D.; Viale, A.; Aime, S. *Chem. Rev.* **2010**, *110*, 3019−3042.

(10) (a) Rinehart, J. D.; Long, J. R. *Chem. Sci.* **2011**, *2*, 2078−2085. (b) Sorace, L.; Benelli, C.; Gatteschi, D. *Chem. Soc. Rev.* **2011**, *40*, 3092−3104. (c) Luzon, J.; Sessoli, R. *Dalton Trans.* **2012**, *41*, 13556−13567. (d) Baldovi, J. J.; Cardona-Serra, S.; Clemente-Juan, J. M.; Coronado, E.; Gaita-Arino, A.; Palii, A. *Inorg. Chem.* **2012**, *51*, 12565−12574. (e) Woodruff, D. N.; Winpenny, R. E. P.; Layfield, R. A. *Chem. Rev.* **2013**, *113*, 5110−5148.

(11) (a) Haase, M.; Schäfer, H. *Angew. Chem., Int. Ed.* **2011**, *50*, 5808−5829. (b) Pansare, V. J.; Hejazi, S.; Faenza, W. J.; Prud'homme, R. K. *Chem. Mater.* **2012**, *24*, 812−827. (c) Liu, Y.; Tu, D.; Zhu, H.; Chen, X. *Chem. Soc. Rev.* **2013**, *42*, 6924−6958.

(12) (a) Kido, J.; Okamoto, Y. *Chem. Rev.* **2002**, *102*, 2357−2368. (b) Evans, R. C.; Douglas, P.; Winscom, C. J. *Coord. Chem. Rev.* **2006**, *250*, 2093−2126. (c) de Bettencourt-Dias, A. *Dalton Trans.* **2007**, 2229−2241. (d) Binnemans, K. *Chem. Rev.* **2009**, *109*, 4283−4374. (e) Katkova, M. A.; Bochkarev, M. N. *Dalton Trans.* **2010**, *39*, 6599−6612. (f) Feng, J.; Zhang, H. *Chem. Soc. Rev.* **2013**, *42*, 387−410.

(13) (a) Stanley, J. M.; Holliday, B. J. *Coord. Chem. Rev.* **2012**, *256*, 1520−1530 and references therein. (b) Liang, H.; Xie, F. *J. Lumin.* **2013**, *144*, 230−233.

(14) (a) Wolf, M. O. *Adv. Mater.* **2001**, *13*, 545−553. (b) Wolf, M. O. *J. Inorg. Organomet. Polym.* **2006**, *16*, 189−199.

(15) (a) Borkovec, M.; Koper, G. J. M. *J. Phys. Chem. B* **1994**, *98*, 6038−6045. (b) Koper, G.; Borkovec, M. *J. Phys. Chem. B* **2001**, *105*, 6666−6674. (c) Koper, G. J. M.; van Duijvenbode, R. C.; Stam, D. P. W.; Steurle, U.; Borkovec, M. *Macromolecules* **2003**, *36*, 2500−2507. (d) Borkovec, M.; Koper, G. J. M.; Piguet, C. *Curr. Opin. Colloid Interface Sci.* **2006**, *11*, 280−289. (e) Koper, G. J. M.; Borkovec, M. *Polymer* **2010**, *51*, 5649−5662.

(16) (a) Piguet, C.; Borkovec, M.; Hamacek, J.; Zeckert, K. *Coord. Chem. Rev.* **2005**, *249*, 705−726. (b) Hamacek, J.; Borkovec, M.; Piguet, C. *Dalton Trans.* **2006**, 1473−1490.

(17) (a) Wyman, J. *J. Mol. Biol.* **1965**, *11*, 631−644. (b) Borkovec, M.; Hamacek, J.; Piguet, C. *Dalton Trans.* **2004**, 4096−4105. (c) Herrera, I.; Winnik, M. A. *J. Phys. Chem. B* **2013**, *117*, 8659−8672.

(18) Piguet, C. *Chem. Commun.* **2010**, *46*, 6209−6231.

(19) Dalla Favera, N.; Hamacek, J.; Borkovec, M.; Jeannerat, D.; Ercolani, G.; Piguet, C. *Inorg. Chem.* **2007**, *46*, 9312−9322.

(20) (a) Aboshyan-Sorgho, L.; Nozary, H.; Aebischer, A.; Bünzli, J.-C. G.; Morgantini, P.-Y.; Kittilstved, K. R.; Hauser, A.; Eliseeva, S. V.; Petoud, S.; Piguet, C. *J. Am. Chem. Soc.* **2012**, *134*, 12675−12684. (b) Le Natur, F.; Calvez, G.; Daiguebonne, C.; Guillou, O.; Bernot, K.; Ledoux, J.; Le Pollès, L.; Roiland, C. *Inorg. Chem.* **2013**, *52*, 6720−6730. (c) Sorensen, T. J.; Tropiano, M.; Blackburn, O. A.; Tilney, J. A.; Kenwright, A. M.; Faulkner, S. *Chem. Commun.* **2013**, *49*, 783−785.

(21) Riis-Johannessen, T.; Dalla Favera, N.; Todorova, T. K.; Huber, S. M.; Gagliardi, L.; Piguet, C. *Chem.—Eur. J.* **2009**, *15*, 12702−12718.

(22) McKenzie, B. M.; Wojtecki, R. J.; Burke, K. A.; Zhang, C.; Jakli, A.; Mather, P. T.; Rowan, S. J. *Chem. Mater.* **2011**, *23*, 3525−3533.

(23) Beck, J. B.; Rowan, S. J. *J. Am. Chem. Soc.* **2003**, *125*, 13922−13923.
(24) (a) Lemonnier, J.-F.; Guénée, L.; Bernardinelli, G.; Vigier, J.-F.; Bocquet, B.; Piguet, C. *Inorg. Chem.* **2010**, *49*, 1252−1265. (b) Lemonnier, J.-F.; Guénée, L.; Beuchat, C.; Wesolowski, T. A.; Mukherjee, P.; Waldeck, D. H.; Gogik, K. A.; Petoud, S.; Piguet, C. *J. Am. Chem. Soc.* **2011**, *133*, 16219−16234. (c) Lemonnier, J.-F.; Babel, L.; L., G.; Mukherjee, P.; Waldeck, D. H.; Eliseeva, S. V.; Petoud, S.; Piguet, C. *Angew. Chem., Int. Ed.* **2012**, *51*, 11302−11305.
(25) (a) Zaïm, A.; Nozary, H.; Guénée, L.; Besnard, C.; Lemonnier, J.-F.; Petoud, S.; Piguet, C. *Chem.—Eur. J.* **2012**, *18*, 7155−7168. (b) Zaïm, A.; Dalla Favera, N.; Guénée, L.; Nozary, H.; Hoang, T. N. Y.; Eliseeva, S. V.; Petoud, S.; Piguet, C. *Chem. Sci.* **2013**, *4*, 1125−1136.
(26) (a) Evans, W. J.; Giarikos, D. G.; Johnston, M. A.; Greci, M. A.; Ziller, J. W. *J. Chem. Soc., Dalton Trans.* **2002**, 520−526. (b) Malandrino, G.; Lo Nigro, R.; Fragalà, I. L.; Benelli, C. *Eur. J. Inorg. Chem.* **2004**, 500−509.
(27) Lima, N. B. D.; Gonçalves, S. M. C.; Junior, S. A.; Simas, A. M. *Sci. Rep.* **2013**, *3*, 2395. DOI: 10.1038/srep02395.
(28) During the titration processes, we detected a minor dependence of the equilibrium ratios $[Ln(\mathbf{L3^{Ph}})]/[Ln]\cdot[\mathbf{L3^{Ph}}]$ on the increase of the product concentrations, a phenomenon reminiscent of the desolvation energy term recently introduced by Castellano, B. M.; Eggers, D. K. *J. Phys. Chem. B* **2013**, *117*, 8180−8188 . This effect is too limited in magnitude for being quantitatively analyzed here because of the experimental uncertainties resulting from the successive addition of small aliquots of volatile $CD_2Cl_2$ solutions. The experimental equilibrium ratios are therefore fitted as fixed conditional stability constants applicable for the specific case of infinite dilution.
(29) Wu, C.-J. J.; Xue, C.; Kuoa, Y.-M.; Luo, F.-T. *Tetrahedron* **2005**, *61*, 4735−4741.
(30) Ward, T. C. *J. Chem. Educ.* **1981**, *58*, 879.
(31) The polydispersity index of the polymer **L4** decreases with the number of successive fractionation procedures and therefore inversely depends on the global yields (see the Experimental Section). An $I_P$ as low as 1.03 could be obtained for yields below 5%, whereas $I_P \gg 1.11$ for 5−10% yields and $I_P \gg 1.3$ for 15−20% yields. We have selected a batch with 18% yield for studying the metal loading process.
(32) Amatore, C.; Le Duc, G.; Jutand, A. *Chem.—Eur. J.* **2013**, *19*, 10082−10093 and references therein..
(33) Willcott, M. R.; Lenkinski, R. E.; Davis, R. E. *J. Am. Chem. Soc.* **1972**, *94*, 1742−1744.
(34) (a) Escande, A.; Guénée, L.; Buchwalder, K.-L.; Piguet, C. *Inorg. Chem.* **2009**, *48*, 1132−1147. (b) Terazzi, E.; Zaïm, A.; Bocquet, B.; Varin, J.; Guénée, L.; Dutronc, T.; Lemonnier, J.-F.; Floquet, S.; Cadot, E.; Heinrich, B.; Donnio, B.; Piguet, C. *Eur. J. Inorg. Chem.* **2013**, 3323−3333.
(35) (a) Nakamoto, K. *J. Phys. Chem.* **1960**, *64*, 1420−1425. (b) Piguet, C.; Bünzli, J.-C. G.; Bernardinelli, G.; Bochet, C. G.; Froidevaux, P. *J. Chem. Soc., Dalton Trans.* **1995**, 83−97. Terazzi, E.; Guénée, L.; Morgantini, P.-Y.; Bernardinelli, G.; Donnio, B.; Guillon, D.; Piguet, C. *Chem.—Eur. J.* **2007**, *13*, 1674−1691.
(36) Piguet, C.; Bocquet, B.; Müller, E.; Williams, A. F. *Helv. Chim. Acta* **1989**, *72*, 323−337.
(37) (a) Bhaumik, M. L. *J. Chem. Phys.* **1964**, *40*, 3711−3715. (b) Binnemans, K. In *Handbook on the Physics and Chemistry of Rare Earths*; Gschneidner, K. A., Bünzli, J.-C. G., Pecharsky, V. K., Eds.; Elsevier North Holland: Amsterdam, 2005; Vol. 35, 107−272. (c) Brito, H. F.; Malta, O. M. L.; Felinto, M. C. F. C.; Teotonio, E. E. S. *The Chemistry of Metal Enolates*; John Wiley & Sons, Ltd: New York, 2009; chapter 3, pp 131−184. (d) Miyata, K.; Hasegawa, Y.; Kuramochi, Y.; Nakagawa, T.; Yokoo, T.; Kawai, T. *Eur. J. Inorg. Chem.* **2009**, 4777−4785. (e) Chen, Z.-N.; Ding, F.; Hao, F.; Guan, M.; Bian, Z.-Q.; Ding, B.; Huang, C.-H. *New J. Chem.* **2010**, *34*, 487−494. (f) Eliseeva, S. V.; Pleshkov, D. N.; Lyssenko, K. A.; Lepnev, L. S.; Bünzli, J.-C. G.; Kuzmina, N. P. *Inorg. Chem.* **2011**, *50*, 5137−5144. (g) Freund, C.; Porzio, W.; Giovanella, U.; Vignali, F.; Pasini, M.; Destri, S.; Mech, A.; Di Pietro, S.; Di Bari, L.; Mineo, P. *Inorg. Chem.* **2011**, *50*, 5417−5429.
(38) Meech, S. R.; Phillips, D. C. *J. Photochem.* **1983**, *23*, 193−217.
(39) Chauvin, A.-S.; Gumy, F.; Imbert, D.; Bünzli, J.-C. G. *Spectrosc. Lett.* **2004**, *37*, 517−532; Erratum **2006**, *40* (1), 193.
(40) Altomare, A.; Burla, M. C.; Camalli, M.; Cascarano, G.; Giacovazzo, C.; Guagliardi, A.; Moliterni, G.; Polidori, G.; Spagna, R. *J. Appl. Crystallogr.* **1999**, *32*, 115−119.
(41) Sheldrick, G. M. *SHELXL97 Program for the Solution and Refinement of Crystal Structures*; University of Göttingen: Göttingen, Germany, 1997.
(42) ORTEP3 for Windows: Farrugia, L. J. *J. Appl. Crystallogr.* **1997**, *30*, 565.